

# Bandwidth enhancement of dual-band bi-directional microstrip antenna using complementary split ring resonator with defected structure for 3/5 GHz applications

Charenrkiat Pochaiya<sup>1</sup>, Srawouth Chandhaket<sup>1</sup>, Prapan Leekul<sup>2</sup>, Jhirat Mearnchu<sup>3</sup>,  
TanawutTantisoparak<sup>4</sup>, Thunyawat Limpiti<sup>5</sup>

<sup>1</sup>School of Engineering and Technology, Walailak University, Nakhon Si Thammarat, Thailand

<sup>2</sup>Faculty of Industrial Technology, RambhaiBarni Rajabhat University, Chanthaburi, Thailand

<sup>3</sup>Faculty of Engineering and Industrial Technology, Silpakorn University, Nakhon Pathom, Thailand

<sup>4</sup>Faculty of Engineering, KhonKaen University, Khonkaen, Thailand

<sup>5</sup>Center of Excellence on Wood and Biomaterials, School of Engineering and Technology, Walailak University, Nakhon Si Thammarat, Thailand

## Article Info

### Article history:

Received Jun 13, 2021

Revised Sep 17, 2021

Accepted Oct 10, 2021

### Keywords:

Bi-directional radiation pattern

Complementary split ring resonator

Defected structure

Dual-band antenna

Microstrip antenna

## ABSTRACT

This paper presents a bandwidth enhancement of a dual-band bi-directional rectangular microstrip patch antenna. The novelty of this work lies in the modification of conventional rectangular microstrip patch antenna by using the combination of two techniques: a complementary split ring resonator (CSRR) and a defected patch structure (DPS). The structure of antenna was studied and investigated via computer simulation technology (CST). The dimension and position of CSRR on the ground plane was optimized to achieve dual bandwidth and bi-directional radiation pattern characteristics. In addition, the bandwidths were enhanced by defecting suitable shape incorporated in the microstrip patch. A prototype with overall dimension of 70.45×63.73 mm<sup>2</sup> has been fabricated on FR-4 substrate. To verify the proposed design, the impedance bandwidth, gain, and radiation patterns were carried out in measurements. The measured impedance bandwidths were respectively 560 MHz (3.08-3.64 GHz) and 950 MHz (4.64-5.59 GHz) while the measured gains of each bandwidth were respectively 4.28 dBi and 4.63 dBi. The measured radiation patterns were in good agreement with simulated ones. The proposed antenna achieves wide dual bandwidth and bi-directional radiation patterns performances. Consequently, it is a promising candidate for Wi-Fi or 5G communications in specific areas such as tunnel, corridor, or transit and rail.

*This is an open access article under the [CC BY-SA](https://creativecommons.org/licenses/by-sa/4.0/) license.*



## Corresponding Author:

Thunyawat Limpiti

School of Engineering and Technology, Walailak University

222Thaiburi Sub-district, Thasala District, Nakhon Si Thammarat80160, Thailand

Email: thunyawat.li@wu.ac.th, limpthu@gmail.com

## 1. INTRODUCTION

Demand of the upcoming technology for the fifth-generation (5G) wireless communication has been rapid increasing due to the inherent advantages of high channel capacity and high data rate communication [1]. To support these capabilities, an antenna with wide bandwidth characteristic is required. There are many wideband or ultra-wideband antennas [2]–[6], but their structures are too bulky. Thus, microstrip patch antenna is one of the most interesting structures that always be chosen to use due to its compact size, light weight, low cost and ease of fabrication and integration [7], [8]. However, its major drawback is narrow

impedance bandwidth, typically less than 5% [9]. Thus, many works concerning how to widen the bandwidth of microstrip patch antenna such as feeding with different techniques or applying material composites have been published. A technique called proximity coupled-feed deals with the feeding mechanism only while the patch structure is still fix. The bandwidth at the order of 8% can be achieved, but the antenna structure is thicker than conventional one [10]. Coupled parasitic elements with shorting vias has been presented in [11]. The antenna structure is only on a single substrate, but the added parasitic elements and vias cause the antenna structure more complex. A differential-fed with shorting posts has been presented, but its feeding network is quite complex [12]. In addition, a technique of defecting patch structure (DPS) with different shapes to create multi-paths of surface current distribution is much interesting since it can increase bandwidth without changing the overall structure [13]–[16]. For example, a d-shaped defected into patch structure can increase bandwidth to 126 MHz [16]. According to aforementioned, they only focused on increasing the impedance bandwidth of a single resonant frequency and remaining the input impedance and the radiation pattern constant over the frequency band. Nevertheless, the designs for fractional bandwidths of microstrip patch antennas are quite a few. Especially the dual-band antennas that having wide bandwidth and bi-directional radiation pattern for using in specific areas such as corridor, tunnel, or transit and rail are still lacking.

In order to increase the multiple resonant frequencies, a complementary split ring resonator (CSRR) is an interesting technique. It has previously been published to enhance microstrip antennas since it not only increases bandwidth and gain but also resonates at multiple frequencies. CSRR is the metamaterial structure which is loading a typical microstrip or coplanar waveguide (CPW) transmission line with reactive elements to generate the artificial substrate that has the simultaneously negative permittivity and permeability. It was originally proposed as a notch filter element in microstrip transmission line [17]. In the recent years, CSRR structure has been extensively developed to enhance microstrip antennas performance and other microwave devices such as microstrip lines, filters, and waveguides [18]–[20]. In addition, it is etched in the ground plane underneath a microstrip feed line to behaves like a tank circuit resonance to convert a single band to dual band microstrip antennas [21]–[24]. However, it is inherent of microstrip patch antenna that provides uni-directional radiation patterns and there are quite a few works involving designs for bi-directional radiation pattern.

In this paper, the bandwidth enhancement of a dual-band bi-directional microstrip patch antenna by using CSRR combined with DPS techniques is proposed. The antenna was initially designed by calculating the dimension of CSRR for embedding it into a rectangular microstrip patch antenna to get dual frequency function. Then, it was modeled in CST simulation software to study and investigate the optimum dimension and position of CSRR on the ground plane. The optimized CSRR configuration that provided dual bandwidth and bi-directional radiation pattern characteristics was then further used in DPS design to enhance the bandwidth and get better impedance matching. The prototype antenna was fabricated and measured impedance bandwidth, gain, and radiation patterns to verify the proposed design.

## 2. RESEARCH METHOD

### 2.1. Antenna design concept and CSRR principle

The optimized configuration of antenna is illustrated in Figure 1. It was designed on a 1.6 mm thick FR-4 substrate which the dielectric constant and the loss tangent are respectively 4.44 and 0.02. The design procedure consists of 3 main steps which initially starts by calculating the dimension of conventional rectangular microstrip patch antenna with a microstrip line feeding at the frequency of 3.1 GHz. The second step is to achieve the second resonant frequency at 5 GHz and bi-directional radiation pattern by embedding CSRR on the ground plane. The Final step is done by defecting on the rectangular patch to increase a number of paths for surface current distribution to widen the bandwidth of the first resonant frequency. All procedures in antenna design are shown in Figure 2.

Split ring resonator (SRR) behaves analogously to an LC resonant circuit. The inductance is created by the circulating current through the rings while the capacitance is generated between gaps and splits of the rings. Due to the complementary nature of Barbinet principle [25], the inductances in SRR become capacitance in CSRR and vice versa to the capacitances. In the design, CSRR is etched on the ground plane beneath the microstrip line feed which is the position causing strong magnetic coupling to achieve a new resonance. The equivalent circuit of CSRR is shown in Figure 3. The operating frequency  $f_r$  is 5 GHz thus the initial dimension of CSRR can be numerically estimate from (1) [26]:

$$f_r = \frac{1}{2\pi\sqrt{L_{res}C_{res}}} \quad (1)$$

where  $L_{res}$  and  $C_{res}$  are respectively the inductance and the capacitance of CSRR which can be obtained from (2),

$$L_{res} = \frac{L_0}{4} \tag{2}$$

$$C_{res} = \frac{\pi^3 \epsilon_0}{c^2} \int_0^\infty \frac{[bB(kb) - aB(ka)]^2}{k^2} \left[ 0.5 \left( 1 + \frac{1 + \frac{\epsilon}{\epsilon_0} \tanh(kh)}{1 + \frac{\epsilon_0}{\epsilon} \tanh(kh)} \right) \right] dk \tag{3}$$

where  $\epsilon, \mu$ , and  $c$  are respectively the permittivity, the permeability, and the velocity of electromagnetic wave. In the design,  $\epsilon$  is the dielectric constant of substrate which equals 4.44. In addition,  $a=r_0 - c/2$  and  $b = c + a$  where  $r_0$  and  $c$  are respectively the radius of CSRR and the slit width.  $B(x)$  can be found in (4),

$$B(x) = S_0(x)J_1(x) - S_1(x)J_0(x) \tag{4}$$

where  $S_n(x)$  and  $J_n(x)$  are respectively the  $n^{\text{th}}$  order Struve function and the Bessel function which can be calculated in (5),

$$S_n(x) = \sum_{m=0}^\infty \frac{(-1)^m}{\Gamma(m+3/2)\Gamma(m+n+3/2)} \left(\frac{x}{2}\right)^{m+1} \tag{5}$$

$$J_n(x) = \left(\frac{x}{2}\right)^n \sum_{m=0}^\infty \frac{\left(\frac{-x^2}{4}\right)^m}{m!\Gamma(n+M+1)} \tag{6}$$

while  $L_0$  can be calculated in (7).

$$L_0 = \frac{\pi^3 \mu_0}{4c^2} \int_0^\infty \frac{[bB(kb) - aB(ka)]^2}{k^2} dk \tag{7}$$

From the expressions, the calculated  $L_{res}$  and  $C_{res}$  in terms of CSRR dimensions:  $c, d, g$ , and  $r_0$  as depicted in Figure 3 are obtained which will be used as initial dimensions to model in simulation.

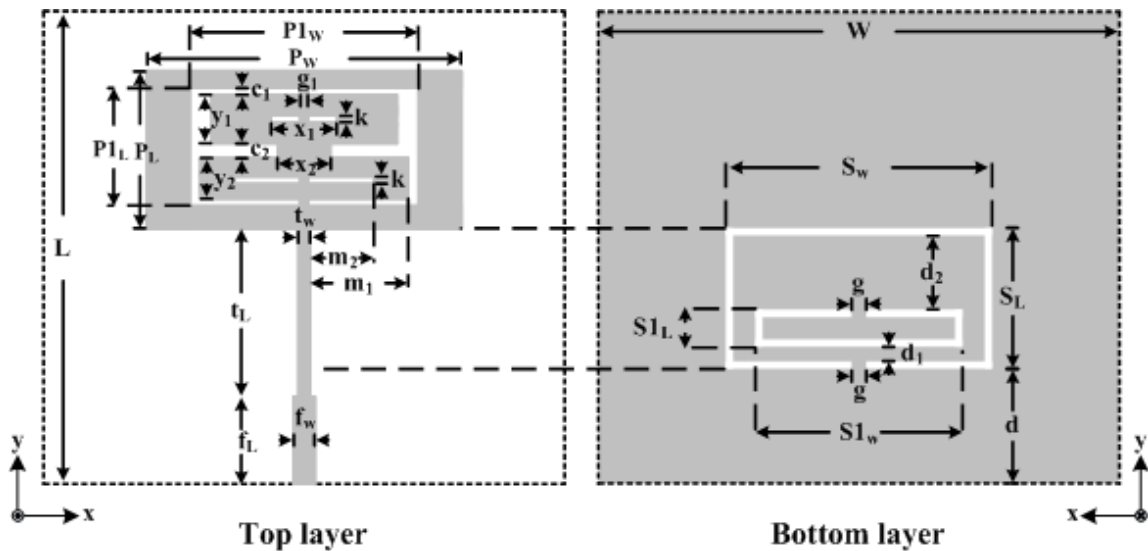


Figure 1. Configuration of proposed bandwidth-enhanced dual-band bi-directional rectangular microstrip antenna

## 2.2. Antenna simulation

The calculated dimensions of CSRR obtained from previous section are modeled in CST Microwave Studio program [27]. In the simulation, the CSRR structure was embedded on the ground plane of rectangular microstrip patch antenna and modified by considering the reflection coefficient  $S_{11}$ .

### 2.2.1. CSRR design

In the simulation, the key parameter that strongly determining the shift of resonant frequency is the width  $S_w$  of the outer square of CSRR. When the slit width of CSRR and the length  $S_L$  are respectively fixed at 1 and 19 mm, it can obviously see in Figure 4 that the resonant frequency shifts to lower frequency as the  $S_w$  increases. The optimum dimensions of outer square of CSRR are  $S_L=19$  mm,  $S_w=38$  mm that provide the impedance bandwidth of the second resonant frequency equal 300 MHz (5.1-5.4 GHz). Note that a resonant frequency around 4 GHz occurs due to the mutual coupling between CSRR and the microstrip line feed.

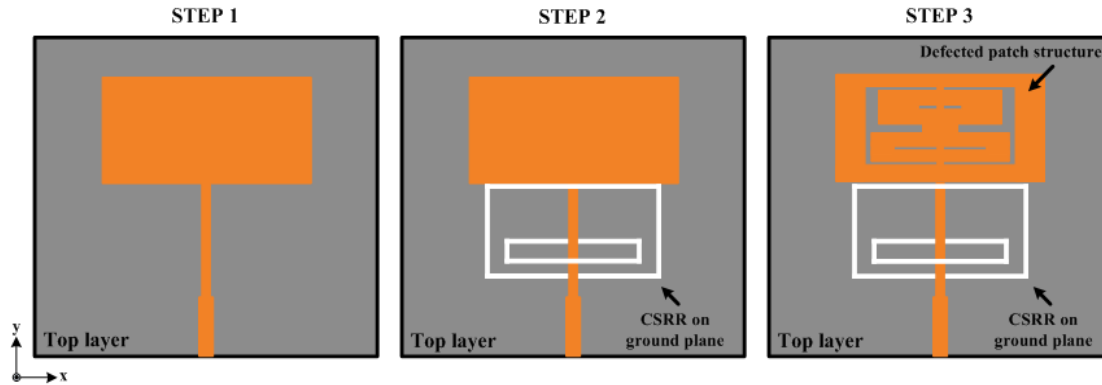


Figure 2. Design procedures of proposed antenna

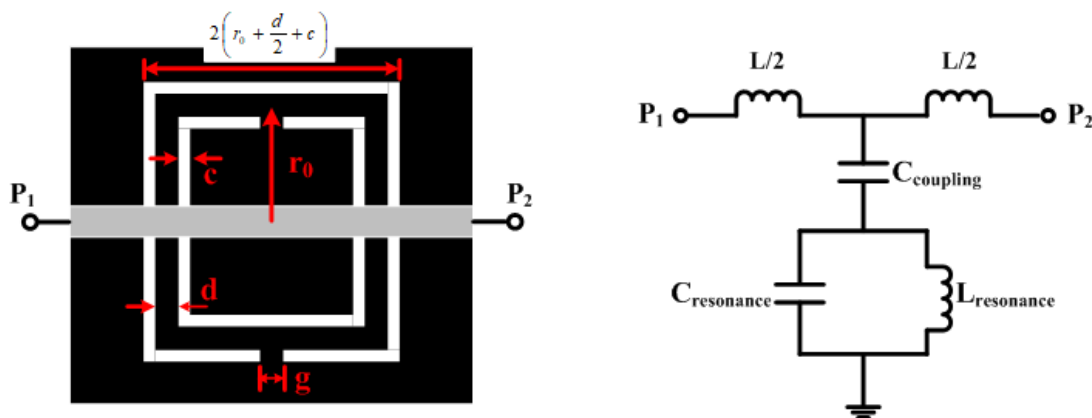


Figure 3. Configuration of CSRR underneath microstrip line feed and equivalent circuit

To widen the bandwidth of second resonant frequency, the length  $S_L$  and the width  $S_w$  of the inner square of CSRR are tuned. In the investigation, the width  $S_w$  is assumed to equal 28 mm and the lengths  $S_L$  are varied in the range of 3-12 mm since the strong coupling between inner and outer squares is near the gap of outer square of CSRR. Thus, the key parameter to resonate the frequency depends on  $S_L$  that causes the CSRR structure be modified by shortening the  $S_L$  to keep the surface wave concentration. It can be obviously noticed in Figure 5 that the bandwidth at 5 GHz is wider as the length  $S_L$  decreases. The surface current distributions on the CSRR configuration at the frequencies of 3.1 and 5 GHz are depicted in Figures 6(a) and 6(b) to better understand. The surface current at 3.1 GHz mainly concentrates around the microstrip patch antenna and CSRR configuration while it concentrates only at the CSRR configuration for the frequency of 5 GHz. In addition, the resonant frequency around 4 GHz still remains, but the  $S_L$  becomes higher. Thus, the CSRR configuration is further tuned in order to suppress the strong coupling between outer square and inner squares of CSRR by adjusting the dimension and the distance of inner and outer squares. The optimum dimensions of CSRR configuration are  $S_L=19$  mm,  $S_w=36$  mm,  $S_L=5$  mm,  $S_w=28$  mm, and  $d_I=2$  mm which the simulated impedance bandwidth obtained from step 2 design procedure is wider than that from step 1 as illustrated in Figure 7. The impedance bandwidth of step 2 is equal to 950 MHz (4.64-5.59 GHz).

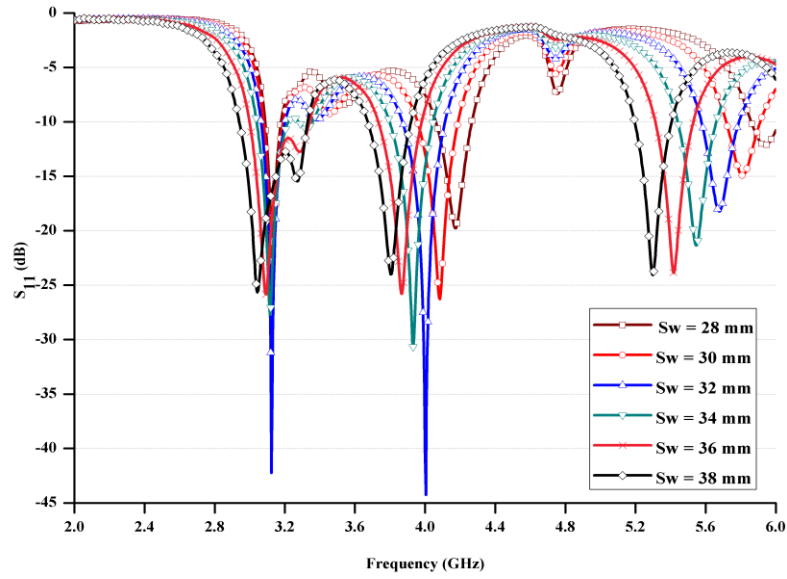


Figure 4. Effect of  $S_w$  on CSRR variation on resonant frequency

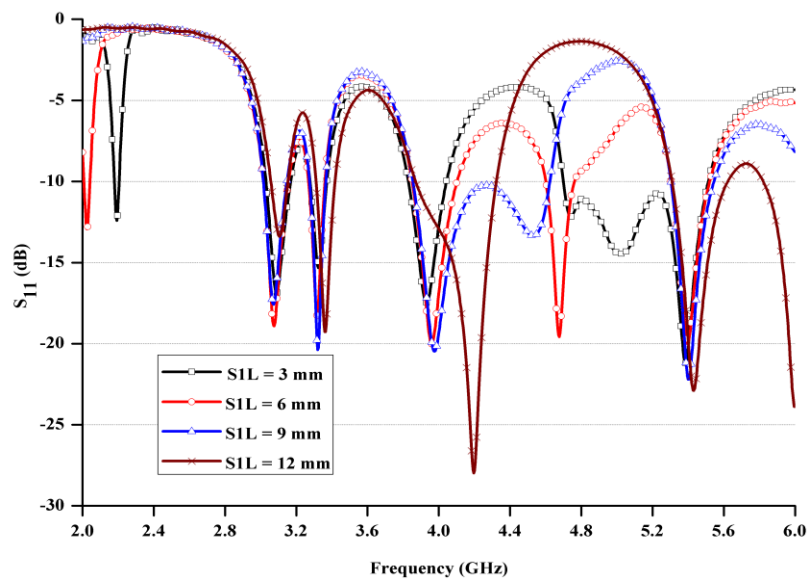


Figure 5. Effect of  $S_{IL}$  on CSRR variation on frequency bandwidth

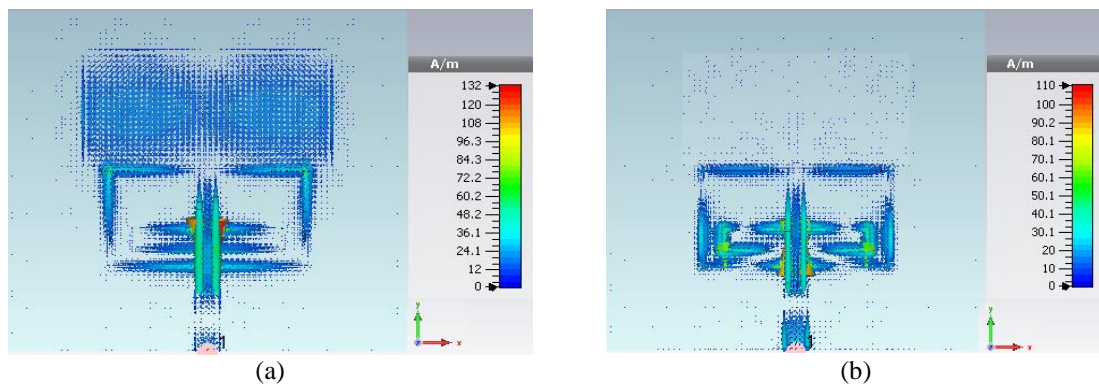


Figure 6. Surface current distribution on antenna design step 2 (a) 3.1 GHz and (b) 5 GHz

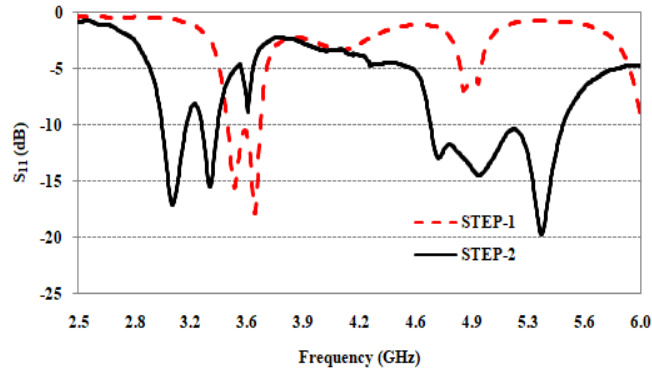


Figure 7. Comparison of simulated  $S_{11}$  of step 1 and step 2 design procedure

### 2.2.2. DPS design

According to the previous subsection, CSRR was added beneath the microstrip line feeding to generate the second resonant frequency. However, the impedance bandwidth of the first resonant frequency is quite narrow. The defecting on patch structure is thus employed in the step 3 design procedure to enhance the bandwidth of the first resonant frequency. It is done on the patch structure where the surface current much concentrates to increase the alternate paths of surface current by discontinuing the distribution from the microstrip line feeding. Firstly, the dumbbell shape is defected to create 3 paths of surface current distribution from the microstrip line feed: the left, the center, and the right paths. Next, the beam of dumbbell shape is unconnected causing the surface current distribution in the center path connects to both the left- and the right-ones so that the double E-shape is formed. Finally, 4 slots are added into the center path of patch structure to create more paths in the center path. All sub-steps of step 3 design procedure are illustrated in Figure 8. For the dumbbell shape defecting, the beam of dumbbell is placed along x-axis which the width  $c_2$  is fixed at 2 mm and the length is then tuned with the width of weight plate shape placed along y-axis. The surface currents distribute along the longest paths, the left- and the right-ones, are unconnected to the center path. In step 3.2 of design procedure, the beam of dumbbell is broken to optimize the width  $x_2$  parameter. In the last step, 4 slots are added to tune the slot lengths and the spacing between slots  $g_1$ . The surface current of DPS design in each step is depicted in Figure 9(a) to Figure 9(c). As clearly seen in step 3.1 design, the surface current distributes near the weight plate shape of dumbbell shape deflection on both left- and right-paths, but the surface current sparsely distributes on the center path. On the step 3.2 design, it can be noticed that the surface current uniformly distributes on all 3 paths as those from the step 3.3 design. However, the surface current distributions from step 3.3 design are denser than those from step 3.2 design.

The simulated  $S_{11}$  results from all sub-steps of step 3 design are compared as illustrated in Figure 10. It can be seen that the impedance bandwidth obtained from step 3.1 is 168 MHz (3.064-3.232 GHz) and it is getting wider to 452 MHz (3.547-3.095 GHz) for the step 3.2. However, the impedance bandwidth of the second resonant compared with that from step 2 decreases from 950 MHz to 595 MHz. The widest impedance bandwidth is obtained from step 3.3 that it increases to 560 MHz (3.08-3.64 GHz) while it slightly affects to the second resonant which decreases to 930 MHz compared with that from step 2. Thus, the optimum dimensions of antenna parameters obtained from the best design are tabulated in Table 1.

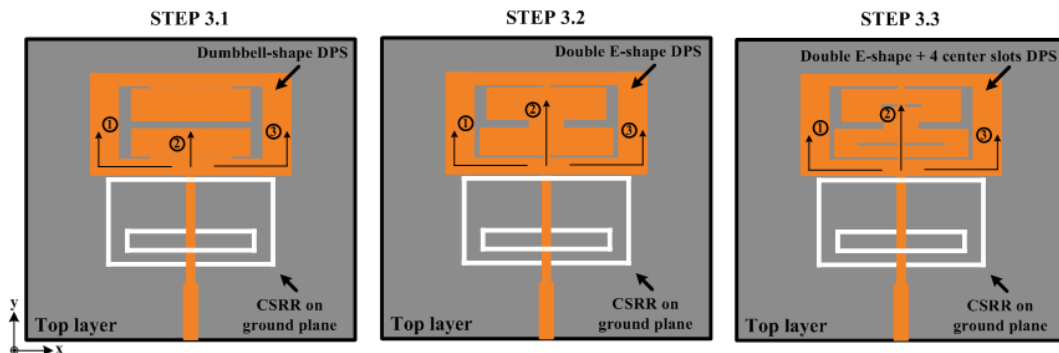


Figure 8. DPS design procedure

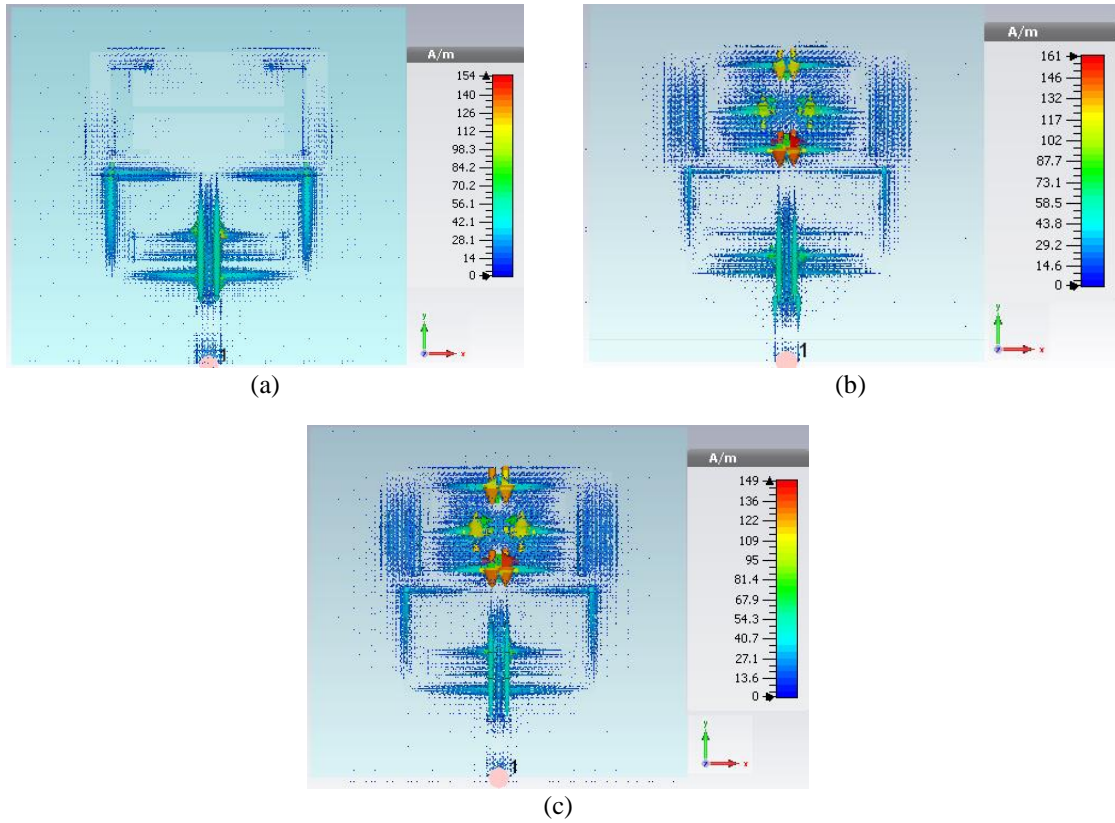


Figure 9. Surface current distribution at 3.1 GHz (a) step 3.1, (b) step 3.2, and (c) step 3.3

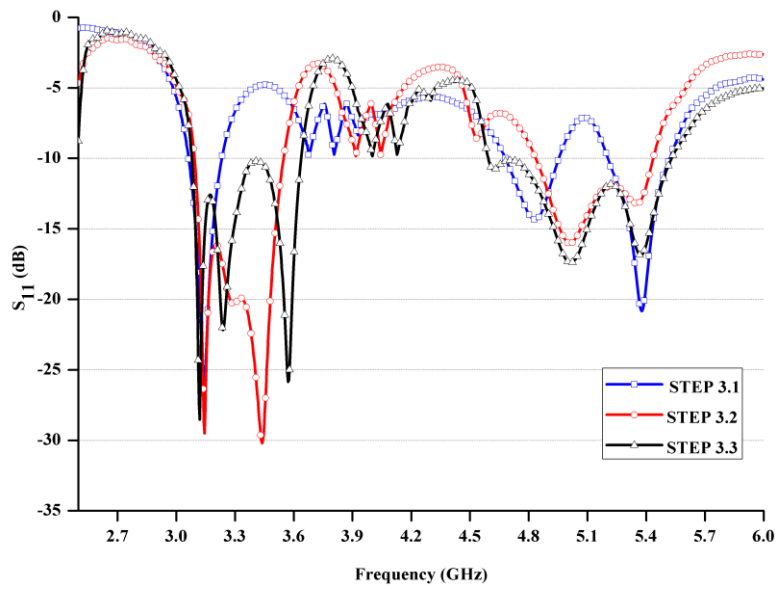


Figure 10. Comparison of simulated  $S_{11}$  of step 3 design procedure

Table 1. Optimum dimensions of design antenna

Parameters	$L$	$W$	$P_L$	$P_w$	$PI_L$	$PI_w$	$g$	$c_2$	$d_1$
Dimension (mm)	63.73	70.45	21.23	42.46	16	31	2	2	2
Parameters	$g_1$	$k$	$c_1$	$x_1$	$x_2$	$y_1$	$y_2$	$m_1$	$m_2$
Dimension (mm)	1	1	1	9	7	6.5	5.5	13.25	8.75
Parameters	$t_L$	$t_w$	$f_L$	$f_w$	$S_L$	$S_w$	$SI_L$	$SI_w$	$d$
Dimension (mm)	22.74	1.5	11.74	2.82	19	36	5	28	15.49

### 3. RESULTS AND DISCUSSION

To validate the antenna design, a prototype antenna has been fabricated on a low-cost FR-4 printed circuit board which is 1.6 mm thick and is excited by a standard 50  $\Omega$  SMA connector. The overall dimension of fabricated antenna is 70.45 mm  $\times$  63.73 mm as depicted in Figures 11(a) and 11(b). On the top plane, the microstrip patch antenna with DPS structure on its structure is connected to the microstrip line feeding while the CSRR structure beneath the microstrip line feeding is on the ground plane.

The experiment was set up to carry out the performance of designed antenna by considering its impedance bandwidth, radiation patterns, and gain. The prototype antenna was connected to a Keysight E5063A network analyzer and then  $S_{11}$  was measured. The measured  $S_{11}$  results compared with simulated results are illustrated in Figure 12. It can be obviously seen that the measured results are in good agreement with the simulated results. The impedance bandwidths of both resonant frequencies around 3.1 GHz and 5 GHz are nearly equal to 560 MHz (3.08-3.64 GHz) and 950 MHz (4.64-5.59 GHz), respectively.



Figure 11. Fabricated antenna, (a) top plane and (b) bottom plane

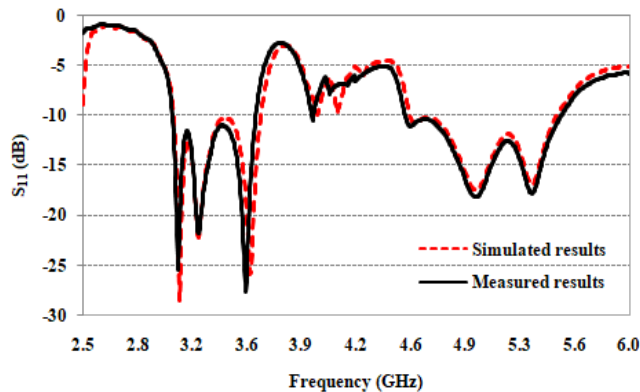


Figure 12. Comparison of simulated and measured  $S_{11}$

The radiation patterns and gain of the designed antenna were also carried out in an anechoic chamber by setting the prototype antenna as the receiving antenna. The SCHWARZBECK USLP 9143 log periodic antenna was exploited as the transmitting antenna which was able to operate cover the frequency range 300 MHz to 7 GHz. Both antennas were placed 8 meters separation which was more than far field range. The radiation patterns were measured both E- ( $\theta=0^\circ$ ) and H- planes ( $\theta=90^\circ$ ) at the center frequency of dual resonant frequencies: 3.36 GHz and 5.1 GHz. They were normalized and compared with simulated results prior to plotting as illustrated in Figures 13(a) and 13(b) for 3.36 GHz while Figures 13(c) and 13(d) were for 5.1 GHz. It can be noticed that the measured radiation patterns in both planes are in good agreement with the simulated results, but there are slightly differences at null position. At the frequency of 3.36 GHz, the 3 dB beamwidth in E-plane is 91 degree and the main lobes point to 0 and 180 degrees, while the 3 dB beamwidth in H-plane is 56 degree and the main lobes point to 224 and 316 degrees. For the frequency of



5.1 GHz, the 3 dB beamwidth in H-plane is 33 degree and the main lobes point to 21 and 159 degrees, but the main lobe in E-plane in the direction of 180 degree is more intense than in the direction of 0 degree. Due to the bi-directional radiation pattern, it can be applied for specific area such as corridor or tunnel as depicted in Figure 14. In addition, the gain of antenna was measured at both resonant frequencies which were respectively 4.28 and 4.63 dBi.

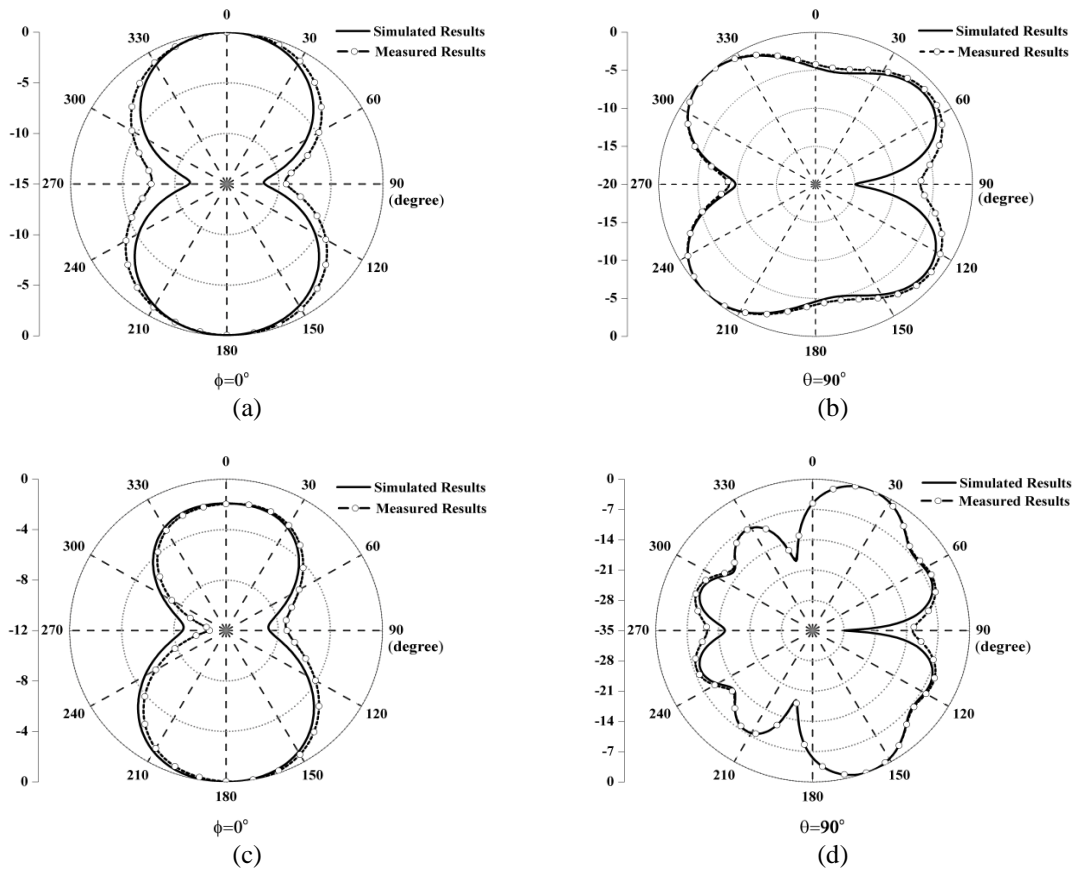


Figure13. Measured radiation patterns: (a) E-plane at 3.36 GHz, (b) H-plane at 3.36 GHz, (c) E-plane at 5.1 GHz, and (d) H-plane at 5.1 GHz

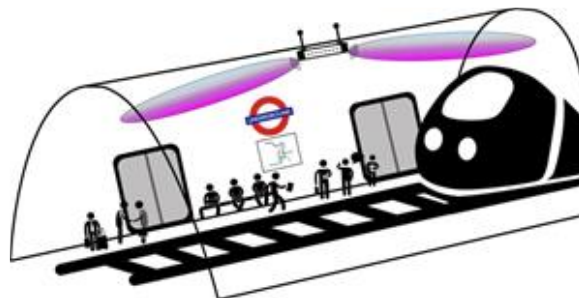


Figure 14. Bi-directional radiation pattern application scenario

#### 4. CONCLUSION

A bandwidth enhancement of dual-band bi-directional rectangular microstrip patch antenna was presented. The novelty of this work is based on the modification of conventional microstrip patch antenna by exploiting the combination of techniques between modified CSRR with DPS. The designed antenna was studied and investigated via CST simulation. The optimized dimension and position of CSRR on the ground plane achieved dual bandwidth and bi-directional radiation pattern characteristics. The strong coupling

occurred in case the CSRR position was beneath the microstrip line feed that also caused the undesired resonant frequency. The CSRR structure was modified to keep the surface current concentration and eliminate undesired resonant frequency by adjust the dimension and the distance of inner and outer-squares of CSRR. Then, the defected suitable shape incorporated in the rectangular patch to enhance the bandwidth. The prototype has been fabricated on a low-cost FR-4 printed circuit board. The performance of designed antenna was carried out in the impedance bandwidth, gain, and radiation patterns measurements. The measured impedance bandwidths were respectively 560 MHz (3.08 to 3.64 GHz) and 950 GHz (4.64 to 5.59 GHz) while the measured gains of each bandwidth were respectively 4.28 and 4.63 dBi. The measured radiation patterns were in good agreement with simulated ones. The proposed antenna achieves wide dual bandwidth and bi-directional radiation patterns performances. Consequently, it is suitable to apply for Wi-Fi or 5G communications for specific areas such as tunnel, corridor, or transit and rail.

## ACKNOWLEDGEMENTS

This work was financial supported by the Thailand Research Fund (TRF) through the MRG Program (Grant MRG6180238). The authors would like to thank A. Jongsuk and T. Preechakarm for prototype of antenna fabrication.




## REFERENCES

- [1] L. Zheng and D. N. C. Tse, "Diversity and multiplexing: A fundamental tradeoff in multiple-antenna channels," *IEEE Transactions on Information Theory*, vol. 49, no. 5, pp. 1073–1096, May 2003, doi: 10.1109/TIT.2003.810646.
- [2] S. Wen and Y. Dong, "A low-profile wideband antenna with monopolelike radiation characteristics for 4G/5G indoor micro base station application," *IEEE Antennas and Wireless Propagation Letters*, vol. 19, no. 12, pp. 2305–2309, Dec. 2020, doi: 10.1109/LAWP.2020.3030968.
- [3] P. D. Kuroptev, V. V. Levyakov, and A. V. Fateev, "Modified 0.6-50 GHz ultra-wideband double-ridged horn antenna design for parameters improvement," in *2017 47th European microwave conference (EuMC)*, Oct. 2017, vol. 2017-Janua, pp. 1313–1316, doi: 10.23919/EuMC.2017.8231093.
- [4] T. Limpiti and A. Y. Chantaveerod, "Design of a printed log-periodic dipole antenna (LPDA) for 0.8–2.5 GHz band applications," in *2016 13th International Conference on Electrical Engineering/Electronics, Computer, Telecommunications and Information Technology (ECTI-CON)*, Jun. 2016, pp. 1–4, doi: 10.1109/ECTICon.2016.7561386.
- [5] X. Tang, Y. He, and B. Feng, "Design of a wideband circularly polarized strip-helical antenna with a parasitic patch," *IEEE Access*, vol. 4, pp. 7728–7735, 2016, doi: 10.1109/ACCESS.2016.2628044.
- [6] T. Yousefi, C. B. Daniel, D. T. Auckland, and R. E. Diaz, "A wideband multimode permeable conformal antenna thinner than  $\lambda/75$  using advanced ferromagnetic laminate composite materials," *IEEE Antennas and Wireless Propagation Letters*, vol. 15, pp. 1931–1934, 2016, doi: 10.1109/LAWP.2015.2512229.
- [7] B. J. Niu and Y. J. Cao, "Bandwidth-enhanced four-antenna MIMO system based on SIW cavity," *Electronics Letters*, vol. 56, no. 13, pp. 643–645, Jun. 2020, doi: 10.1049/el.2020.0799.
- [8] H. Huang, X. Li, and Y. Liu, "A low-profile, single-ended and dual-polarized patch antenna for 5G application," *IEEE Transactions on Antennas and Propagation*, vol. 68, no. 5, pp. 4048–4053, May 2020, doi: 10.1109/TAP.2019.2948743.
- [9] K. F. Lee and K. F. Tong, "Microstrip patch antennas," in *Handbook of Antenna Technologies*, vol. 2, London: Imperial College Press, 2016, pp. 787–852.
- [10] V. Rathi, G. Kumar, and K. P. Ray, "Improved coupling for aperture coupled microstrip antennas," *IEEE Transactions on Antennas and Propagation*, vol. 44, no. 8, pp. 1196–1198, 1996, doi: 10.1109/8.511831.
- [11] K. Da Xu, H. Xu, Y. Liu, J. Li, and Q. H. Liu, "Microstrip patch antennas with multiple parasitic patches and shorting vias for bandwidth enhancement," *IEEE Access*, vol. 6, pp. 11624–11633, 2018, doi: 10.1109/ACCESS.2018.2794962.
- [12] J. Wang, Q. Liu, and L. Zhu, "Bandwidth enhancement of a differential-fed equilateral triangular patch antenna via loading of shorting posts," *IEEE Transactions on Antennas and Propagation*, vol. 65, no. 1, pp. 36–43, Jan. 2017, doi: 10.1109/TAP.2016.2630660.
- [13] G. F. Khodaei, J. Nourinia, and C. Ghobadi, "A practical miniaturized U-slot patch antenna with enhanced bandwidth," *Progress In Electromagnetics Research B*, vol. 3, pp. 47–62, 2008, doi: 10.2528/ pier07112201.
- [14] R. Chair, C. L. Mak, K. F. Lee, K. M. Luk, and A. A. Kishk, "Miniature wide-band half U-slot and half E-shaped patch antennas," *IEEE Transactions on Antennas and Propagation*, vol. 53, no. 8, pp. 2645–2652, Aug. 2005, doi: 10.1109/TAP.2005.851852.
- [15] S. Weigand, G. H. Huff, K. H. Pan, and J. T. Bernhard, "Analysis and design of broad-band single-layer rectangular U-slot microstrip patch antennas," *IEEE Transactions on Antennas and Propagation*, vol. 51, no. 3, pp. 457–468, Mar. 2003, doi: 10.1109/TAP.2003.809836.
- [16] W. You, H. Guo, W. Cai, and X. Liu, "A D-shaped defected patch antenna with enhanced bandwidth," in *Proceedings - 2009 3rd IEEE International Symposium on Microwave, Antenna, Propagation and EMC Technologies for Wireless Communications, MAPE 2009*, Oct. 2009, pp. 684–686, doi: 10.1109/MAPE.2009.5355654.
- [17] F. Falcone, T. Lopetegi, J. D. Baena, R. Marqués, F. Martín, and M. Sorolla, "Effective negative- $\epsilon$  stopband microstrip lines based on complementary split ring resonators," *IEEE Microwave and Wireless Components Letters*, vol. 14, no. 6, pp. 280–282, Jun. 2004, doi: 10.1109/LMWC.2004.828029.
- [18] F. Alizadeh, C. Ghobadi, J. Nourinia, and R. Zayer, "Bandwidth enhancement of patch antennas loaded with complementary split-ring resonators," in *2014 7th International Symposium on Telecommunications, IST 2014*, Sep. 2014, pp. 224–229, doi: 10.1109/ISTEL.2014.7000702.
- [19] L. Su, J. Naqui, J. Mata-Contreras, and F. Martín, "Modeling and applications of metamaterial transmission lines loaded with pairs of coupled complementary split-ring resonators (CSRRs)," *IEEE Antennas and Wireless Propagation Letters*, vol. 15, pp. 154–157, 2016, doi: 10.1109/LAWP.2015.2435656.




- [20] J. Wang, H. Ning, and L. Mao, "A compact reconfigurable bandstop resonator using defected ground structure on coplanar waveguide," *IEEE Antennas and Wireless Propagation Letters*, vol. 11, pp. 457–459, 2012, doi: 10.1109/LAWP.2012.2196251.
- [21] Y. Xie, L. Li, C. Zhu, and C. Liang, "A novel dual-band patch antenna with complementary split ring resonators embedded in the ground plane," *Progress in Electromagnetics Research Letters*, vol. 25, pp. 117–126, 2011, doi: 10.2528/PIERL11062802.
- [22] L. Meng, L. Mingzhi, and J. C. Tie, "Novel miniaturized dual band antenna design using complementary metamaterial," in *META08 - Proceedings of the 2008 International Workshop on Metamaterials*, Nov. 2008, pp. 374–376, doi: 10.1109/META.2008.4723618.
- [23] N. Ortiz, F. Falcone, and M. Sorolla, "Dual band patch antenna based on complementary rectangular split-ring resonators," in *APMC 2009 - Asia Pacific Microwave Conference 2009*, Dec. 2009, pp. 2762–2765, doi: 10.1109/APMC.2009.5385367.
- [24] H. Zhang, Y. Q. Li, X. Chen, Y. Q. Fu, and N. C. Yuan, "Design of circular/dual-frequency linear polarization antennas based on the anisotropic complementary split ring resonator," *IEEE Transactions on Antennas and Propagation*, vol. 57, no. 10 PART 2, pp. 3352–3355, Oct. 2009, doi: 10.1109/TAP.2009.2029400.
- [25] F. Falcone *et al.*, "Babinet principle applied to the design of metasurfaces and metamaterials," *Physical Review Letters*, vol. 93, no. 19, Nov. 2004, doi: 10.1103/PhysRevLett.93.197401.
- [26] S. Goswami, K. Sarmah, A. Sarma, K. K. Sarma, and S. Baruah, "Design considerations pertaining to the application of complementary split ring resonators in microstrip antennas," IGI Global, 2018, pp. 25–56.
- [27] Sigma Solutions, *CST Microwave Studio*. 2019.

## BIOGRAPHIES OF AUTHORS






**Charernkiat Pochaiya**    was born in Nakhonsithammarat, Thailand, in 1975. He received the B.S. degree in Telecommunication Engineering and M.S. degree in Electrical Engineering from King Mongkut's Institute of Technology Ladkrabang (KMITL), Bangkok, Thailand in 2000 and 2002, respectively and the Ph.D. degree in Electronic Engineering from University of Reading, U.K. in 2018. Since 2008, he has been Assistant Professor in the Electrical Engineering Department, School of Engineering and Technology, Walailak University, Nakhonsithammarat, Thailand. His research interest areas are mobile communication network, telecommunication network and transmission and propagation path-loss models.






**Srawouth Chandhaket**    was born in Surin, Thailand. He received his Bachelor of Electronics from Kobe University, Japan in 1995. He completed his Master of Science in the field of electrical engineering from Virginia Tech in 1998 and Doctor of Engineering from Yamaguchi University in 2004 respectively. He joined the Faculty of Engineering, Walailak University, in 2004 as a lecturer. His research interests are electromagnetic applications, wireless power transmission, electronics circuits design and advanced control for EV.






**Prapan Leekul**    (M'16) was born in Chonburi, Thailand, in 1980. He received the B.Eng. and M.Eng. degrees in telecommunication engineering and D.Eng. degrees in electrical engineering from the King Mongkut's Institute of Technology Ladkrabang (KMITL), Bangkok, Thailand, in 2005, 2008, and 2016, respectively. He is currently an Assistant Professor with the Faculty of Industrial Technology, Rambhai Barni Rajabhat University, His research interests are microwave sensor design, artificial neural networks design, and field programmable gate array.






**Jhirat Mearnchu**    conducted research in developing embedded system and digital electronic. His research interests include developing non-destructive measurement systems for dielectric material. His teaching interests include classes in Sensors, Transducers, Microcontroller and Electronics.



**Tanawut Tantisopharak**    (S'14–M'16) received the B.Eng., M.Eng. degrees in telecommunication engineering and D.Eng. degree in electrical engineering from King Mongkut's Institute of Technology Ladkrabang (KMITL), Bangkok, Thailand, in 2005, 2009 and 2015, respectively. He was a visiting research scholar at the department of electrical engineering and computer science, Syracuse University, Syracuse, NY, USA in 2011. He is currently a lecturer at Department of Electrical Engineering, Faculty of Engineering, Khon Kaen University. His research interests are adaptive antennas, microwave engineering, and electromagnetic wave for agricultural application.



**Thunyawat Limpiti**    (M'10) was born in Phatthalung, Thailand, in 1982. He received the B.Eng. and M.Eng. degrees in telecommunication engineering and D.Eng. degree in electrical engineering from the King Mongkut's Institute of Technology Ladkrabang (KMITL), Bangkok, Thailand, in 2005, 2008, and 2013, respectively. He is currently an Assistant Professor at School of Engineering and Technology, Walailak University. His research interests are in reconfigurable antenna design, microwave sensor design, and microwave techniques for dielectric properties determination.